nature energy

SUPPLEMENTARY INFORMATION

https://doi.org/10.1038/s41560-019-0355-9

In the format provided by the authors and unedited.

Chemical and structural origin of lattice oxygen oxidation in Co–Zn oxyhydroxide oxygen evolution electrocatalysts

Zhen-Feng Huang[1], Jiajia Song[2,3], Yonghua Du[4], Shibo Xi[4], Shuo Dou[1], Jean Marie Vianney Nsanzimana[1], Cheng Wang[5], Zhichuan J. Xu[2]* and Xin Wang[1]*

[1]School of Chemical and Biomedical Engineering, Nanyang Technological University, Singapore, Singapore. [2]School of Materials Science and Engineering, Nanyang Technological University, Singapore, Singapore. [3]Singapore-HUJ Alliance for Research and Enterprise, NEW-CREATE Phase II, Campus for Research Excellence and Technological Enterprise (CREATE), Singapore, Singapore. [4]Institute of Chemical and Engineering Sciences, A*STAR, Singapore, Singapore. [5]Institute for New Energy Materials and Low-Carbon Technologies, Tianjin University of Technology, Tianjin, China. *e-mail: xuzc@ntu.edu.sg; WangXin@ntu.edu.sg

Supplementary Methods

Free energy calculations. The Gibbs free energy changes for the water oxidation steps using AEM and LOM mechanisms were calculated using the following Equations (S1-S5) and (S6-10), respectively[1,2].

$$\Delta G_1 = \Delta G_{O*} - \Delta G_{OH*} - eU + \Delta G_{pH} \text{ (S1)}$$

$$\Delta G_2 = \Delta G_{OOH*} - \Delta G_{O*} - eU + \Delta G_{pH} \text{ (S2)}$$

$$\Delta G_3 = \Delta G_{OO*} - \Delta G_{OOH*} - eU + \Delta G_{pH} \text{ (S3)}$$

$$\Delta G_4 = 4.92 \text{ eV} - \Delta G_{OO*} \text{ (S4)}$$

$$\Delta G_5 = \Delta G_{OH*} - eU + \Delta G_{pH} \text{ (S5)}$$

$$\Delta G_1 = \Delta G_{[OO+O_v]*} - \Delta G_{OH*} - eU + \Delta G_{pH} \text{ (S6)}$$

$$\Delta G_2 = \Delta G_{[OO+H^v]*} - \Delta G_{[OO+O_v]*} - eU + \Delta G_{pH} \text{ (S7)}$$

$$\Delta G_3 = 4.92 \text{ eV} + \Delta G_{[O_v+H^v]*} - \Delta G_{[OO+H^v]*} \text{ (S8)}$$

$$\Delta G_4 = \Delta G_{[OH*+H^v]} - \Delta G_{[O_v+H^v]*} - eU + \Delta G_{pH} \text{ (S9)}$$

$$\Delta G_5 = \Delta G_{OH*} - \Delta G_{[OH*+H^v]} - eU + \Delta G_{pH} \text{ (S10)}$$

where U is the potential measured against normal hydrogen electrode (NHE) at standard condition (T = 298.15 K, P = 1 bar, pH = 0)[3]. The free energy change of the protons relative to the above-specified electrode at non-zero pH is represented by Nernst equation as $\Delta G_{pH} = -k_B T \ln(10) \times \text{pH}$. The Gibbs free energy differences of these intermediates include zero-point energy (ZPE) and entropy corrections (listed in Supplementary Table 7) according to $\Delta G_i = \Delta E_i + \Delta ZPE_i - T\Delta S_i$, where the energy differences ΔE_i are calculated with respect to H_2O and H_2 (at U = 0 and pH = 0). The theoretical overpotential is defined as the lowest potential at which all reaction steps are thermodynamically downhill[1,4].

Supplementary Tables

Supplementary Table 1 | Computed magnetization moments of oxygen ions in CoO_2 and Zn-substituted CoO_2.

Oxygen configuration	CoO_2 (μ_B)	$Zn_{0.1}Co_{0.9}O_2$ (μ_B)	$Zn_{0.2}Co_{0.8}O_2$ (μ_B)	$Zn_{0.5}Co_{0.5}O_2$ (μ_B)
O1		0.062		
		0.064		
	0.047	0.078		
	0.047	0.062		
	0.047	0.063		
	0.047	0.028	0.168	
	0.047	0.029	0.168	
	0.047	0.055		
	0.047	0.042		
	0.047	0.074		
		0.042		
		0.052		
O2		0.261	0.213	
		0.268	0.212	0.162
		0.265	0.212	0.163
		0.257	0.213	0.162
		0.183	0.212	0.163
		0.179	0.212	
O3				0.418
				0.419
				0.418
				0.419

Supplementary Table 2 | Zn/(Zn+Co) mole ratios in ZnCo-MOFs[a], $Zn_xCo_{1-x}OOH$[b] and cycled $Zn_xCo_{1-x}OOH$[c] determined by inductive coupled plasma atomic emission spectrometer.

x in Zn_xCo_{1-x}-MOFs	mole [Zn/(Zn+Co)][a]	mole [Zn/(Zn+Co)][b]	mole [Zn/(Zn+Co)][c]
0	0	0	0
0.1	0.11	0.11	0.12
0.2	0.21	0.19	0.19
0.3	0.30	0.29	0.29
0.4	0.39	0.38	0.38
0.5	0.51	0.45	0.41

Supplementary Table 3 | Fitted parameters of Co K-edge EXAFS curves for CoOOH and $Zn_xCo_{1-x}OOH$. ([a]R: bond distance; [b]CN: coordination numbers; [c]σ^2: Debye-Waller factors; [d]S_0^2: Amplitude attenuation factors.)

Samples	bond	[a]R (Å)	[b]CN	[c]σ^2 (×10^3, Å^2)	[d]S_0^2
CoOOH	Co-O	1.90	6.0 (fixed)	1.6 (fixed)	0.78
$Zn_{0.1}Co_{0.9}OOH$	Co-O	1.89	5.3	1.6 (fixed)	0.78
$Zn_{0.2}Co_{0.8}OOH$	Co-O	1.89	5.1	1.6 (fixed)	0.78
$Zn_{0.3}Co_{0.7}OOH$	Co-O	1.89	5.1	1.6 (fixed)	0.78

Supplementary Table 4 | Oxygen vacancy concentration (δ), Co^{4+} concentration (y) and Co oxidation state (ρ) in $Zn^{2+}_{x}Co^{3+}_{1-x-y}Co^{4+}_{y}O_{2-\delta}H$. (Note the data of δ were calculated based on three iodimetry experiments.)

x in $Zn^{2+}_{x}Co^{3+}_{1-x-y}Co^{4+}_{y}O_{2-\delta}H$	δ	y	ρ
0	0.01	0	2.98
0.1	0.03	0.04	3.04
0.2	0.06	0.08	3.10
0.3	0.08	0.14	3.20
0.4	0.09	0.22	3.36
0.5	0.1	0.3	3.60

Supplementary Table 5 | BET surface areas of $Zn_{x}Co_{1-x}OOH$.

x in $Zn_{x}Co_{1-x}OOH$	BET surface areas (m^2g^{-1})	Pore volume (cm^3g^{-1})
0	91	0.87
0.1	82	0.78
0.2	86	0.81
0.3	65	0.54
0.4	71	0.63
0.5	63	0.51

Supplementary Table 6 | Comparisons of OER performance for various transition metal-based electrocatalysts.

Catalyst	Electrolyte	Substrate	Overpotential at 10 mA cm^{-2} (mV)	References
$Zn_{0.2}Co_{0.8}OOH$	**1 M KOH**	**GCE**	**235**	**This work**
Gelled FeCoW	1 M KOH	GCE	223	*Science* **352**, 333-337 (2016).
ECA-Ni	1 M KOH	Ni foam	210	*Angew. Chem. Int. Ed.* **56**, 5061-5065 (2017).
Au-NiFeOOH	1 M KOH	GCE	237	*J. Am. Chem. Soc.* **140**, 3876-3879 (2018).

CoOOH	1 M KOH	GCE	300	*Nat. Mater.* 11, 550-557 (2012).
γ-CoOOH	1 M KOH	GCE	330	*Angew. Chem. Int. Ed.* **54**, 8722-8727 (2015).
FeOOH/Co/FeOOH	1 M NaOH	Ni foam	240[a]	*Angew. Chem. Int. Ed.* **55**, 3694-3698 (2016).
$Ni_xFe_{1-x}Se_2$-DO		Ni foam	195	*Nat. Commun.* **7**, 12324 (2016).
NiFe LDH/GO	1 M KOH	GCE	210	*ACS Nano* **9**, 1977-1984 (2015).
Ultrathin FeCo LDH	1 M KOH	GCE	290	*Adv. Mater.* DOI: 10.1002/adma.201701546.
NiCo-UMOFNs	1 M KOH	GCE	250	*Nat. Energy*, **1**, 16181 (2016).
Ce-doped NiO_x	1 M NaOH	Au coated GCE	271	*Nat. Energy* **1**, 16053 (2016).
NiFe-MOF	0.1 M KOH	Ni foam	240	*Nat. Commun.* **8**, 15341 (2017).
$Li_{1-x}CoO_2$	0.1 M KOH	CFP	390	*J. Am. Chem. Soc.* **139**, 6270-6276 (2017).
Co_3O_4	0.1 M KOH	FTO	350	*J. Am. Chem. Soc.* **138**, 36-39 (2016).
A-$CoS_{4.6}O_{0.6}$	1 M KOH	GCE	290	*Angew. Chem. Int. Ed.* **56**, 4858-4861 (2017).

Supplementary Table 7 | The calculated zero-point energy and entropy correction values (in eV).

	E	ZPE	TS	G
H_2	-6.99	0.28	0.40	-7.12
H_2O	-14.15	0.57	0.58	-14.17

Supplementary Figures

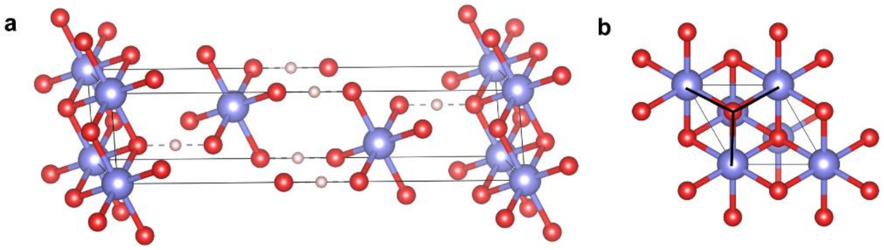

Supplementary Figure 1 | Bulk models of MOOH with side view (a) and top view (b). (Purple, red and pink balls represent M, O and H atoms, respectively.)

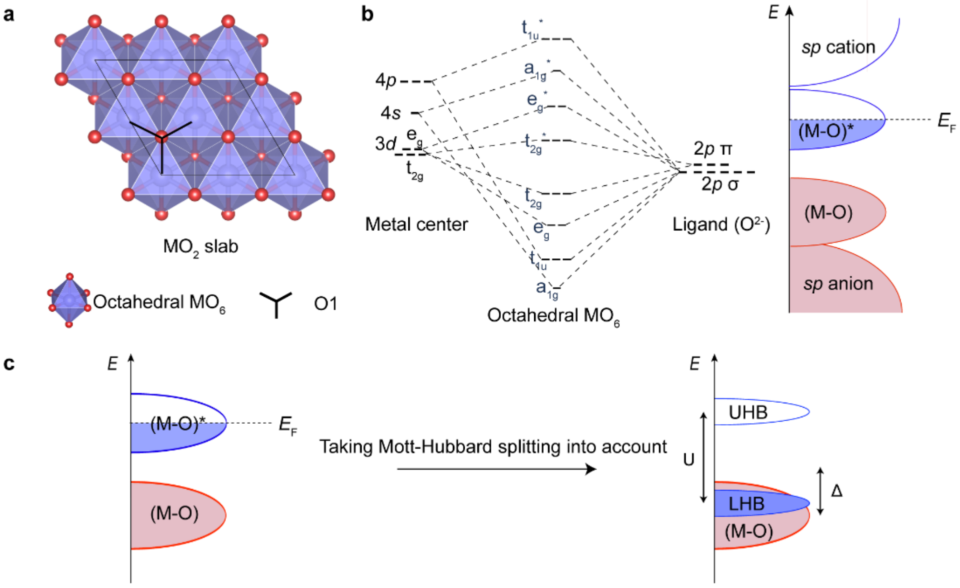

Supplementary Figure 2 | (a) Model and (b) the corresponding band structure of MO_2 slab from the aspect of molecular orbital principles. (c) Schematic energy band in consideration of Mott-Hubbard splitting.

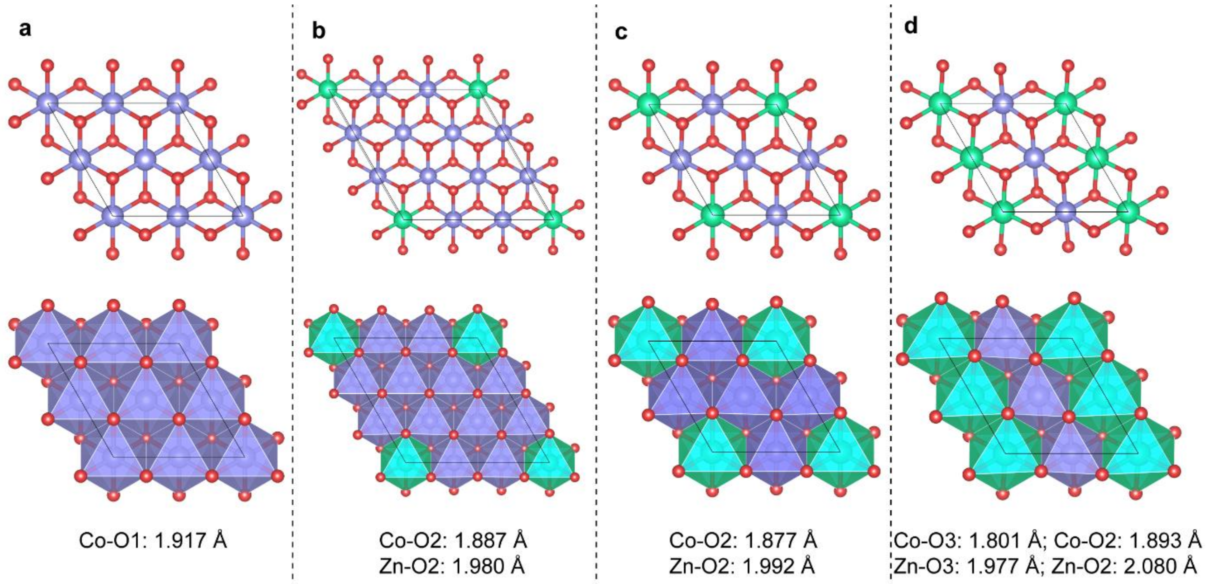

Supplementary Figure 3 | Slab models of CoO_2 and Zn-substituted CoO_2 (a: CoO_2; b: $Zn_{0.1}Co_{0.9}O_2$; c: $Zn_{0.2}Co_{0.8}O_2$; d: $Zn_{0.5}Co_{0.5}O_2$). (Purple, green and red balls represent Co, Zn and O atoms, respectively.)

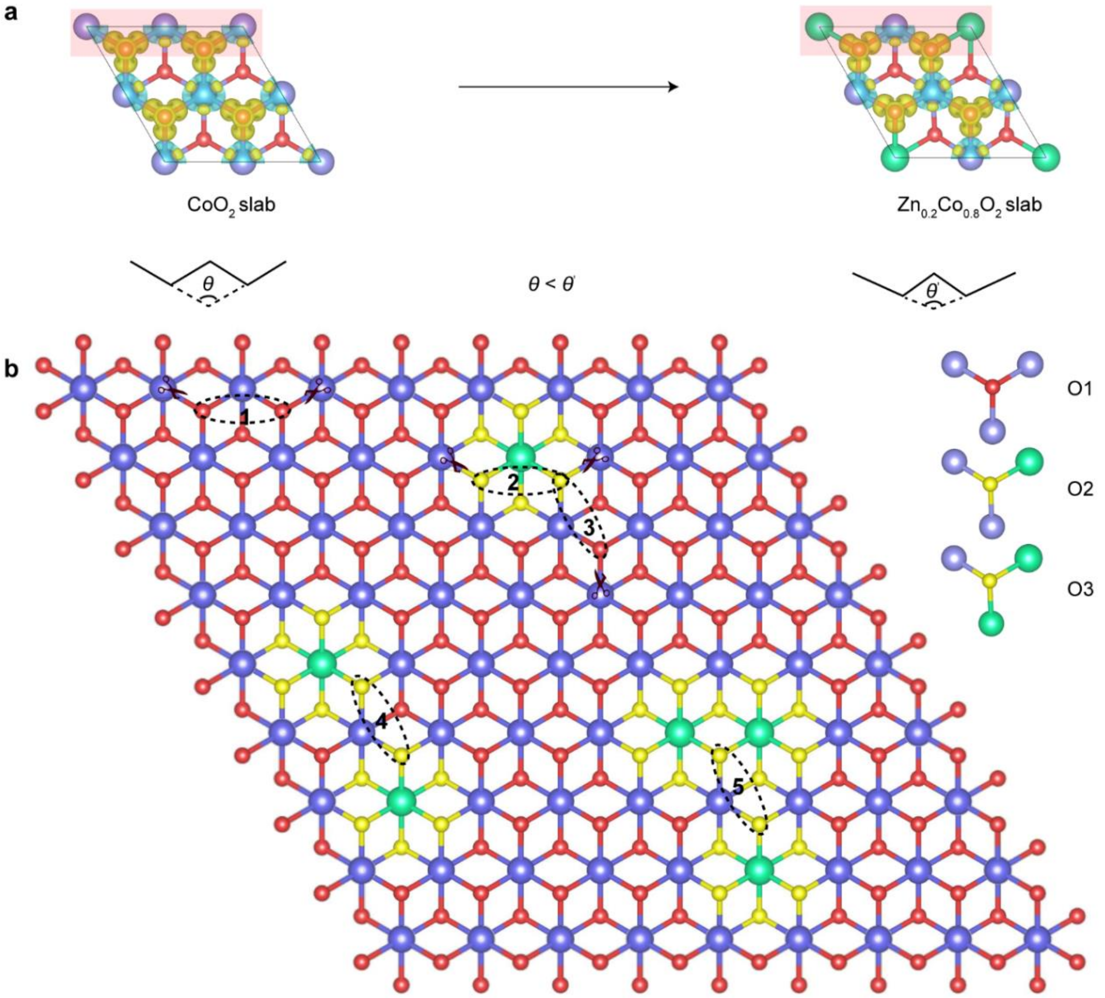

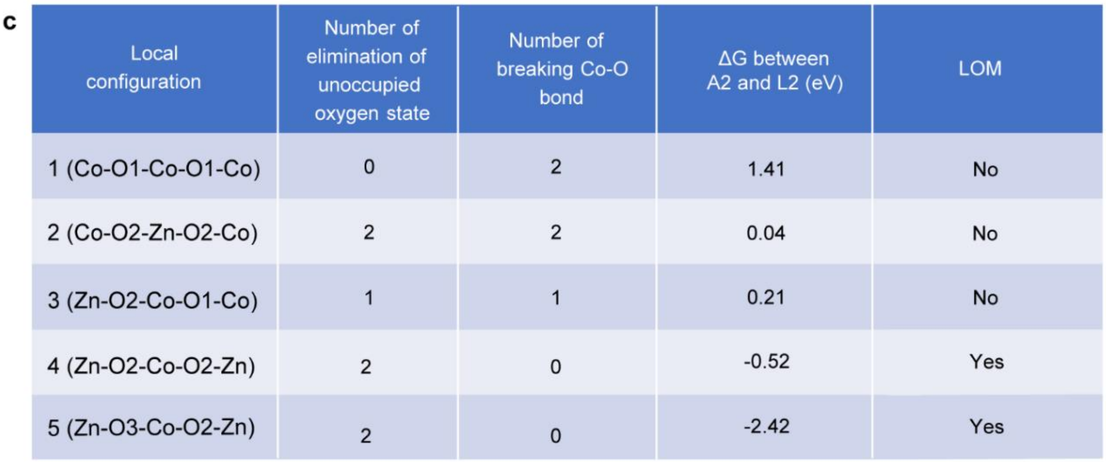

Local configuration	Number of elimination of unoccupied oxygen state	Number of breaking Co-O bond	ΔG between A2 and L2 (eV)	LOM
1 (Co-O1-Co-O1-Co)	0	2	1.41	No
2 (Co-O2-Zn-O2-Co)	2	2	0.04	No
3 (Zn-O2-Co-O1-Co)	1	1	0.21	No
4 (Zn-O2-Co-O2-Zn)	2	0	-0.52	Yes
5 (Zn-O3-Co-O2-Zn)	2	0	-2.42	Yes

Supplementary Figure 4 | (a) Comparison of the intersection angle between two neighboring oxygen ions in CoO_2 and Zn-substituted CoO_2 slabs. (b) Possible local configurations for direct O-O coupling in Zn-substituted CoO_2 slabs (Yellow balls represent as the non-bonded oxygen with oxygen hole.). (c) Comparison of different local configurations to proceed LOM by analyzing both the number of elimination unoccupied oxygen states and the breaking Co-O bonds.

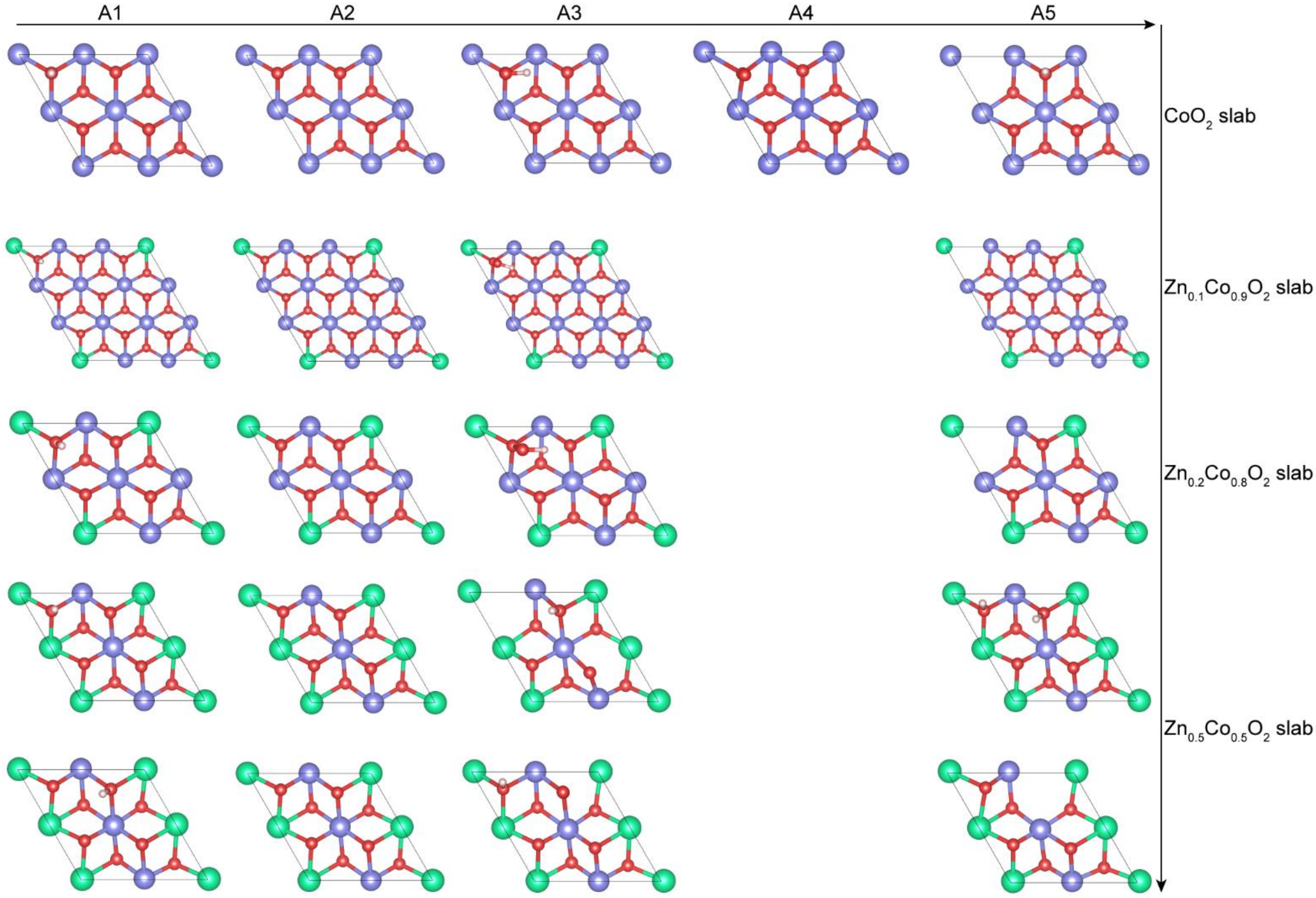

Supplementary Figure 5 | Adsorption models of CoO_2 and Zn-substituted CoO_2 with AEM pathway.

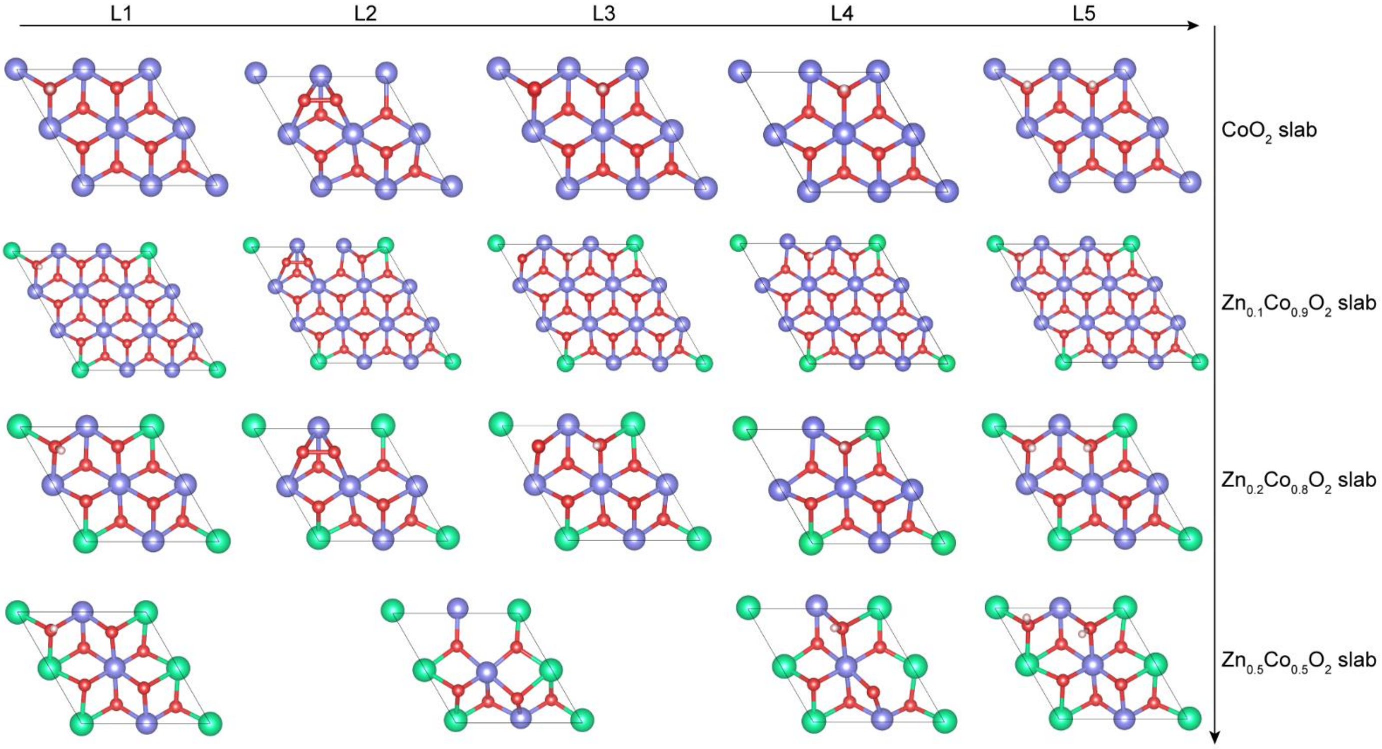

Supplementary Figure 6 | Adsorption models of CoO$_2$ and Zn-substituted CoO$_2$ with LOM pathway.

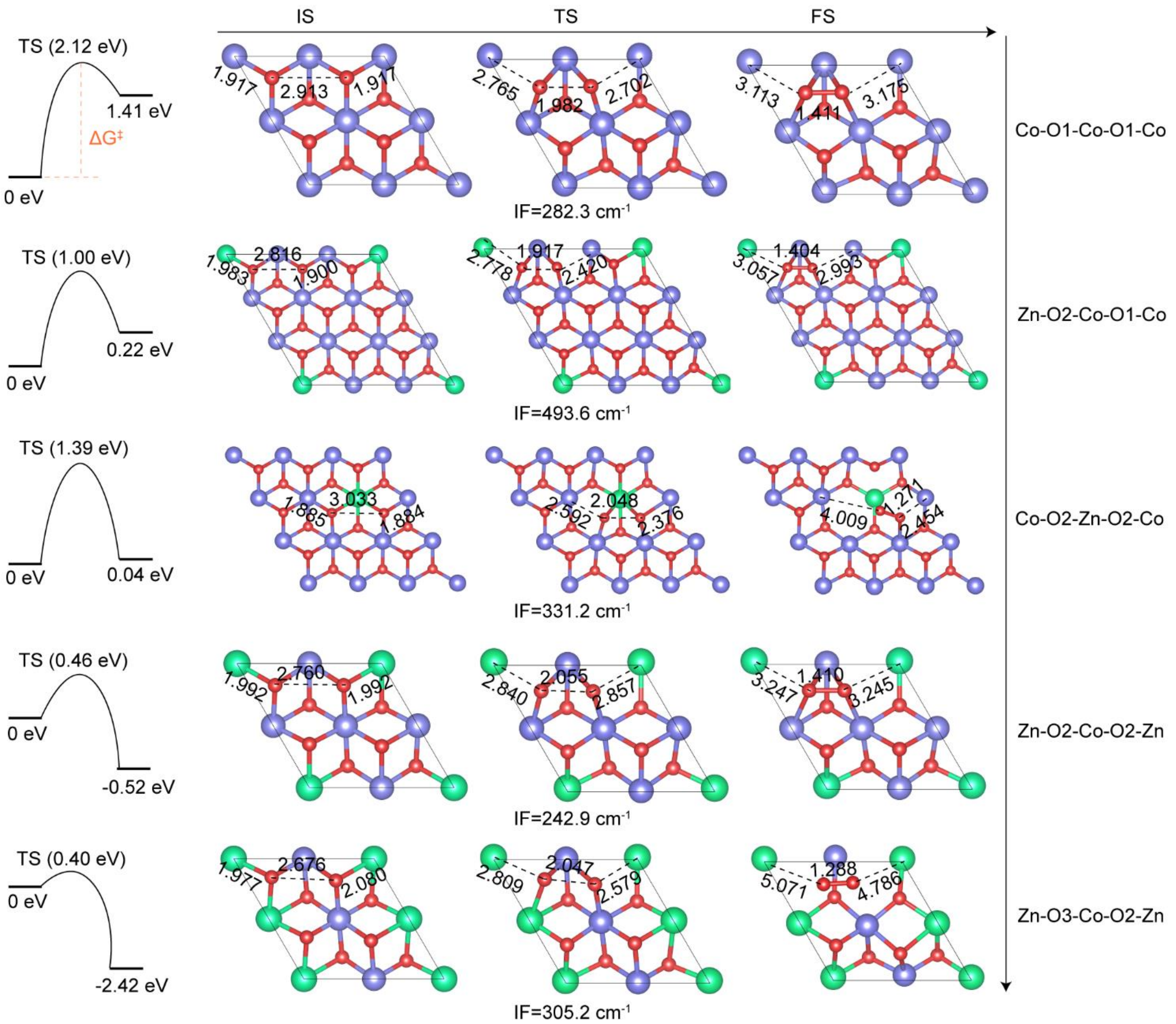

Supplementary Figure 7 | Activation free energy ($\Delta G^{\ddagger}$) for O-O bond formation and corresponding adsorption and transition state structures on CoO_2 and Zn-substituted CoO_2. (IS: initial state; TS: transition state; FS: final state; IF: imaginary frequency; the unit of bond length is Å.)

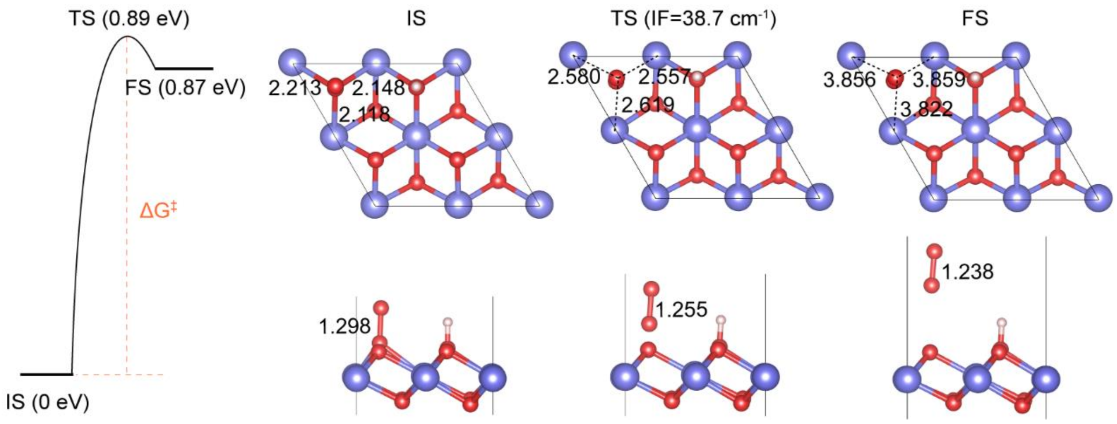

Supplementary Figure 8 | Activation free energy ($\Delta G^{\ddagger}$) for O_2 release and corresponding adsorption and transition state structures in LOM pathway on CoO_2 (IS: initial state; TS: transition state; FS: final state; IF: imaginary frequency; the unit of bond length is Å.).

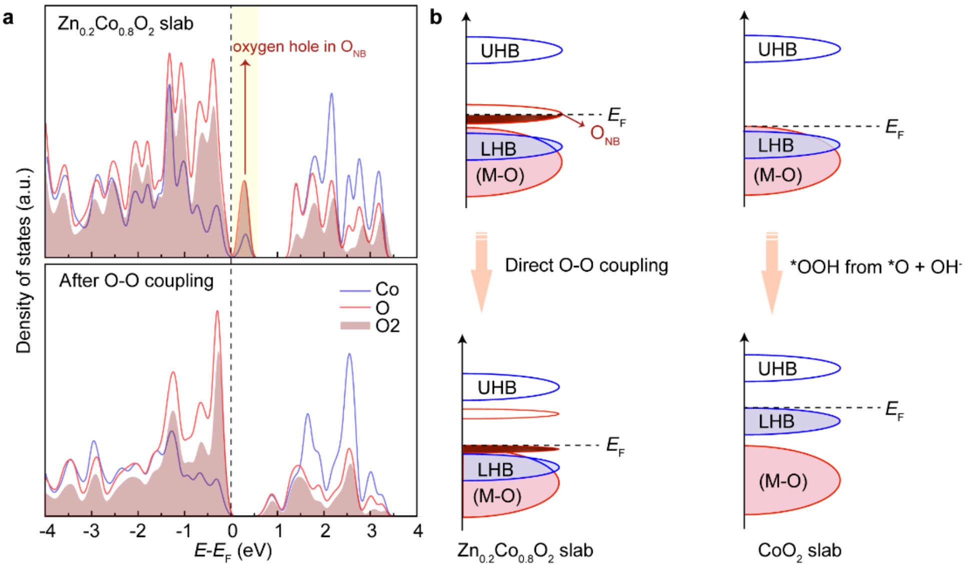

Supplementary Figure 9 | (a) Projected density of states of O(2*p*) and Co(3*d*) orbitals in L2 and A2 intermediate for $Zn_{0.2}Co_{0.8}O_2$. (b) Schematic OER process for CoO_2 and $Zn_{0.2}Co_{0.8}O_2$ following up AEM and LOM pathways, respectively.

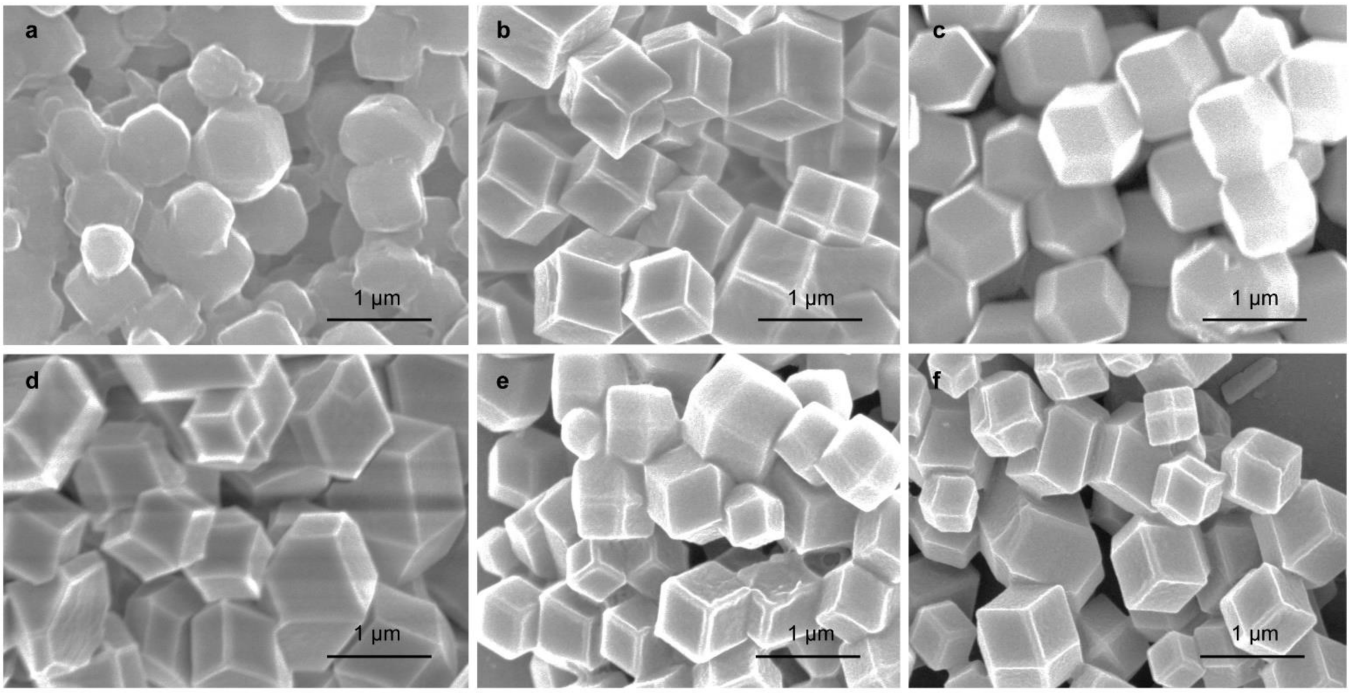

Supplementary Figure 10 | SEM images of ZIF-67 (a) and ZnCo-MOFs (b-f). (b-f: *x* = 0.1, 0.2, 0.3, 0.4 and 0.5).

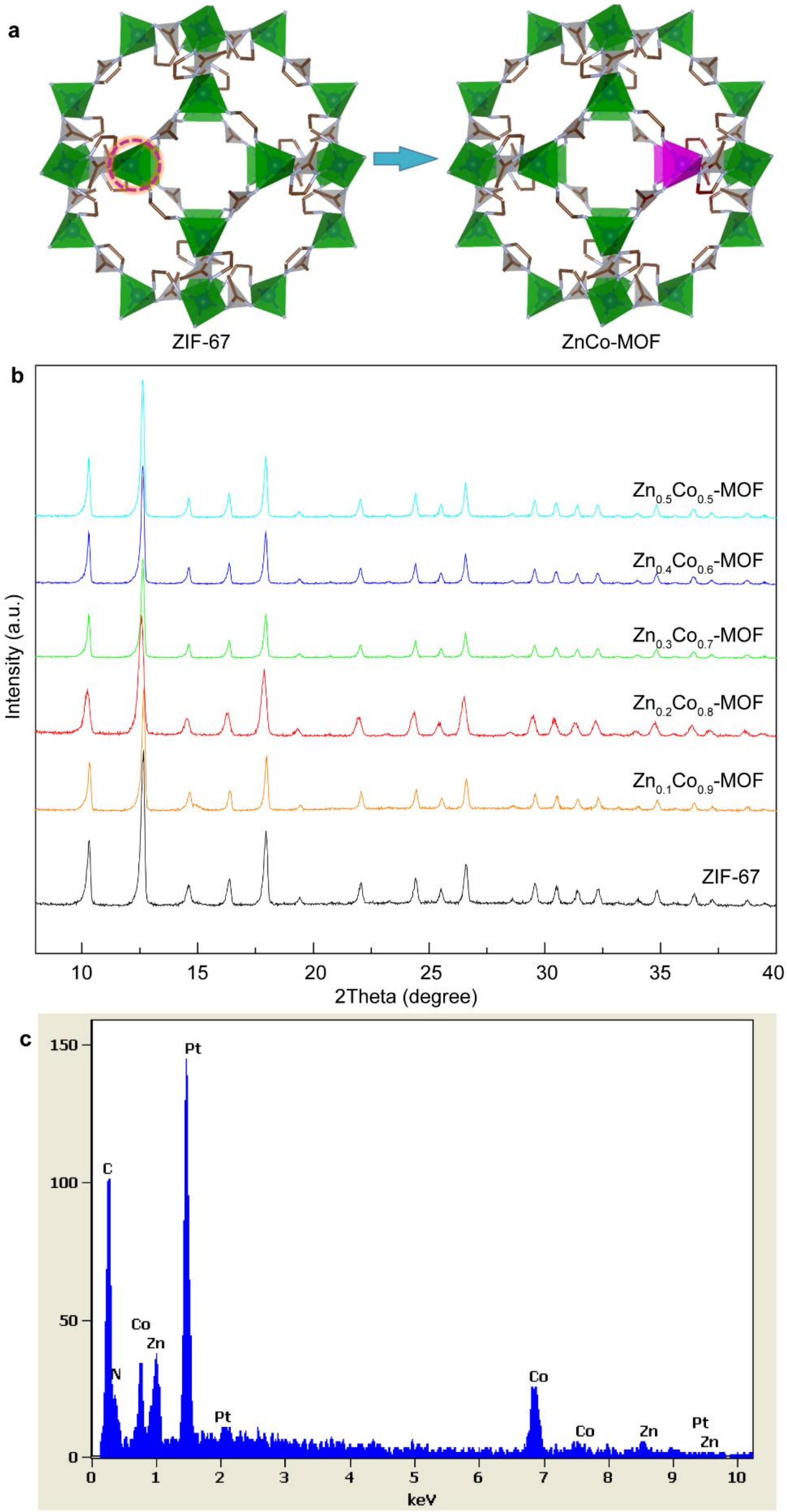

Supplementary Figure 11 | (a) Schematic models of ZIF-67 and ZnCo-MOFs. (b) XRD patterns of ZIF-67 and ZnCo-MOFs. (c) EDS spectrum of $Zn_{0.2}Co_{0.8}$-MOFs.

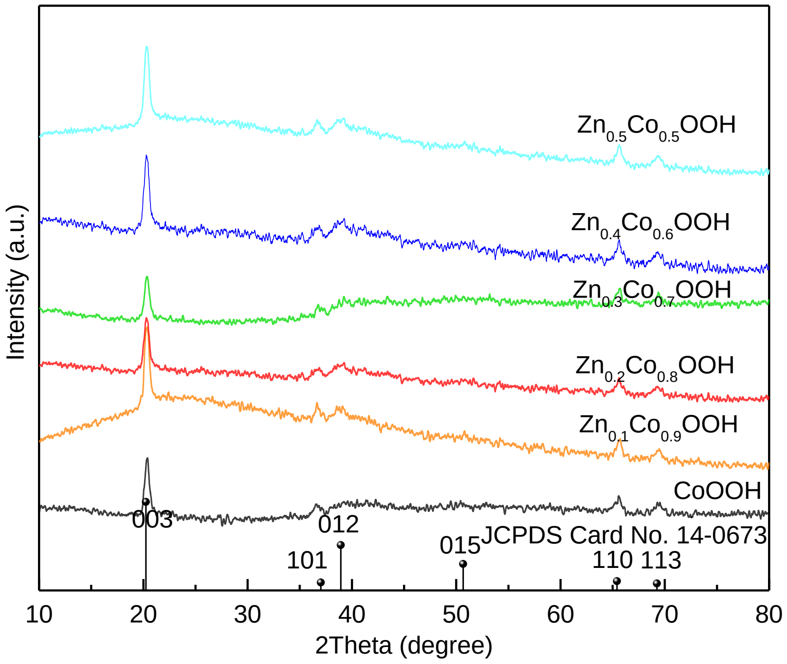

Supplementary Figure 12 | XRD patterns of CoOOH and Zn-substituted CoOOH samples.

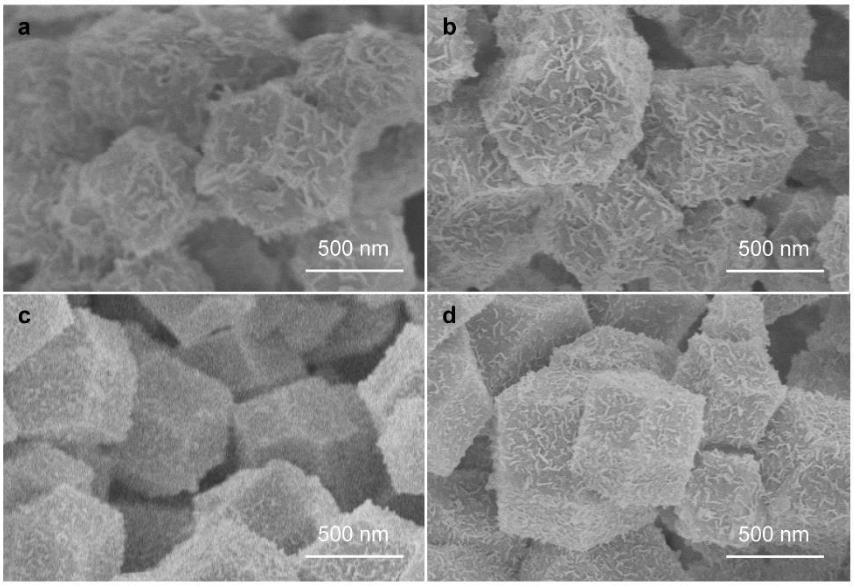

Supplementary Figure 13 | SEM images of $Zn_{0.1}Co_{0.9}OOH$ (a), $Zn_{0.3}Co_{0.7}OOH$ (b), $Zn_{0.4}Co_{0.7}OOH$ (c) and $Zn_{0.5}Co_{0.5}OOH$ (d).

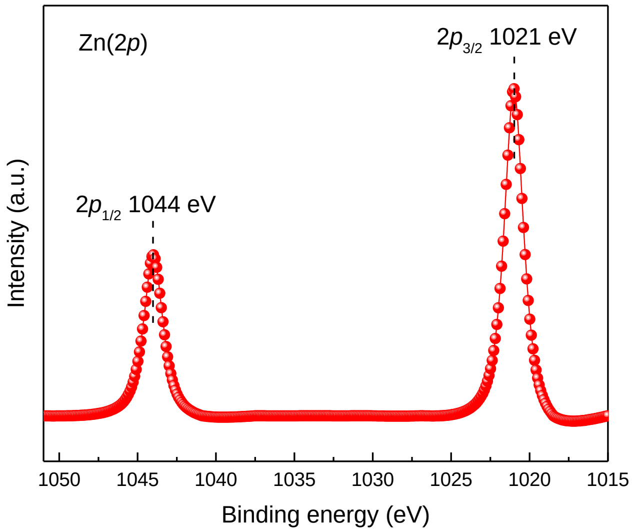

Supplementary Figure 14 | Zn(2*p*) XPS spectrum of $Zn_{0.2}Co_{0.8}OOH$.

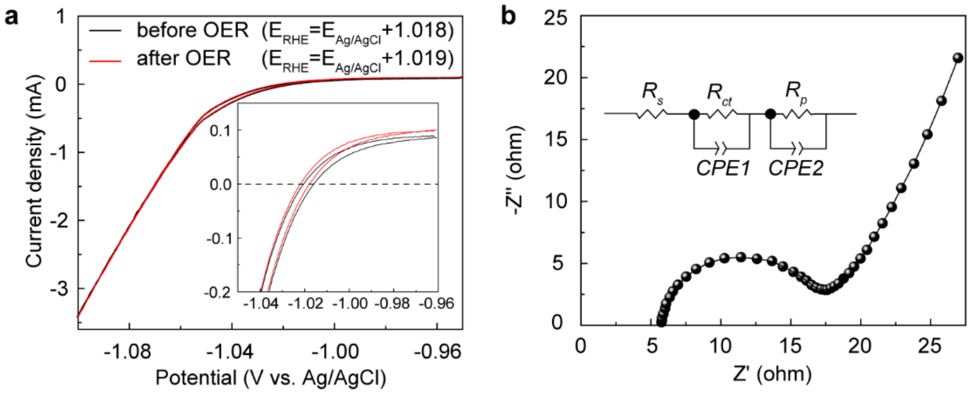

Supplementary Figure 15 | (a) Reversible hydrogen electrode (RHE) calibration. (b) solution resistance measurement. Calibration of the Ag/AgCl reference electrode was conducted in the standard three-electrode system at ambient temperature using 40 wt% Pt/C (0.204 mg cm^{-2}) and Pt foils as the working and counter electrodes at a rotational speed of 1600 rpm.

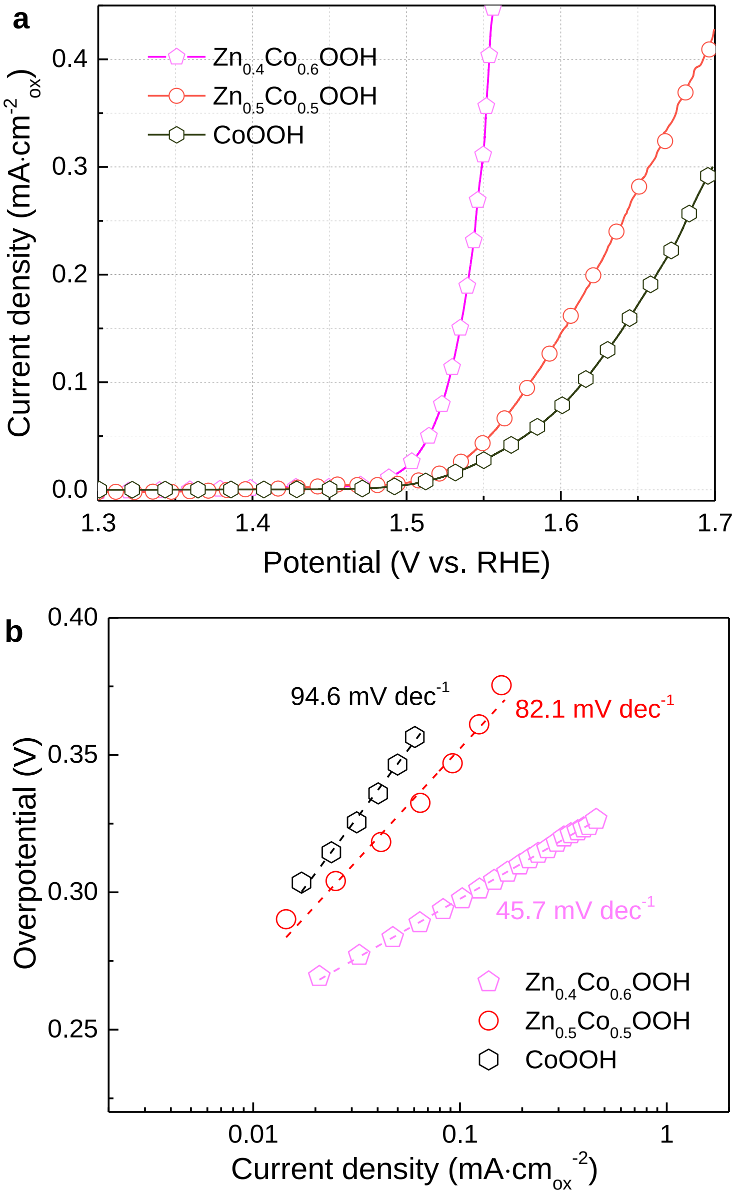

Supplementary Figure 16 | Polarization curves (a) and corresponding Tafel plots (b) of Zn-substituted CoOOH ($x = 0.4$ and 0.5) with pure CoOOH as comparison.

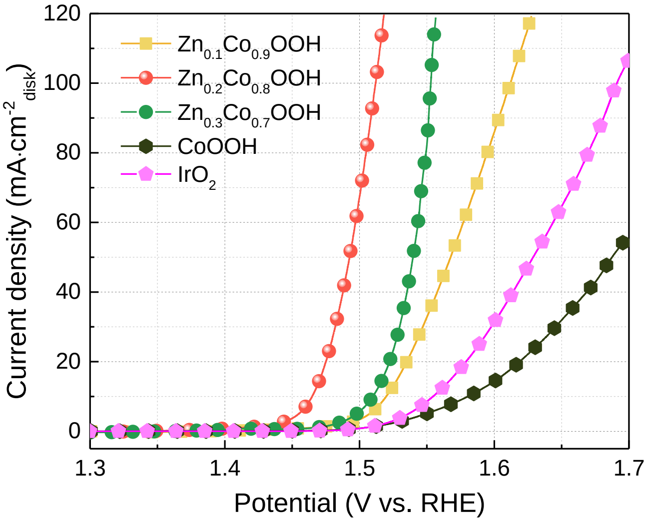

Supplementary Figure 17 | Polarization curves of Zn-substituted CoOOH (x = 0, 0.1, 0.2 and 0.3) with IrO_2 as comparision.

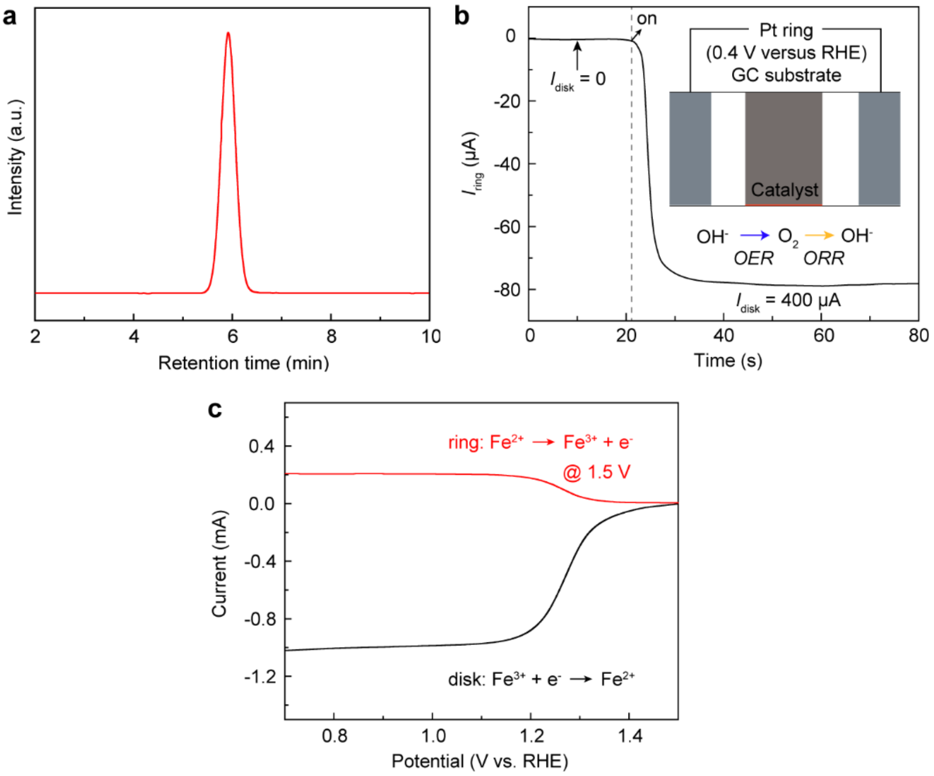

Supplementary Figure 18 | Faraday efficiency testing of $Zn_{0.2}Co_{0.8}OOH$ at the current density of 20 mA cm^{-2} using the GC (a) and RRDE (b) technique in N_2-saturated 1 M KOH solution. RRDE evaluation for collection efficiency in N_2-purged 1.0 M KOH containing 10 mM $K_3Fe(CN)_6$ (c).

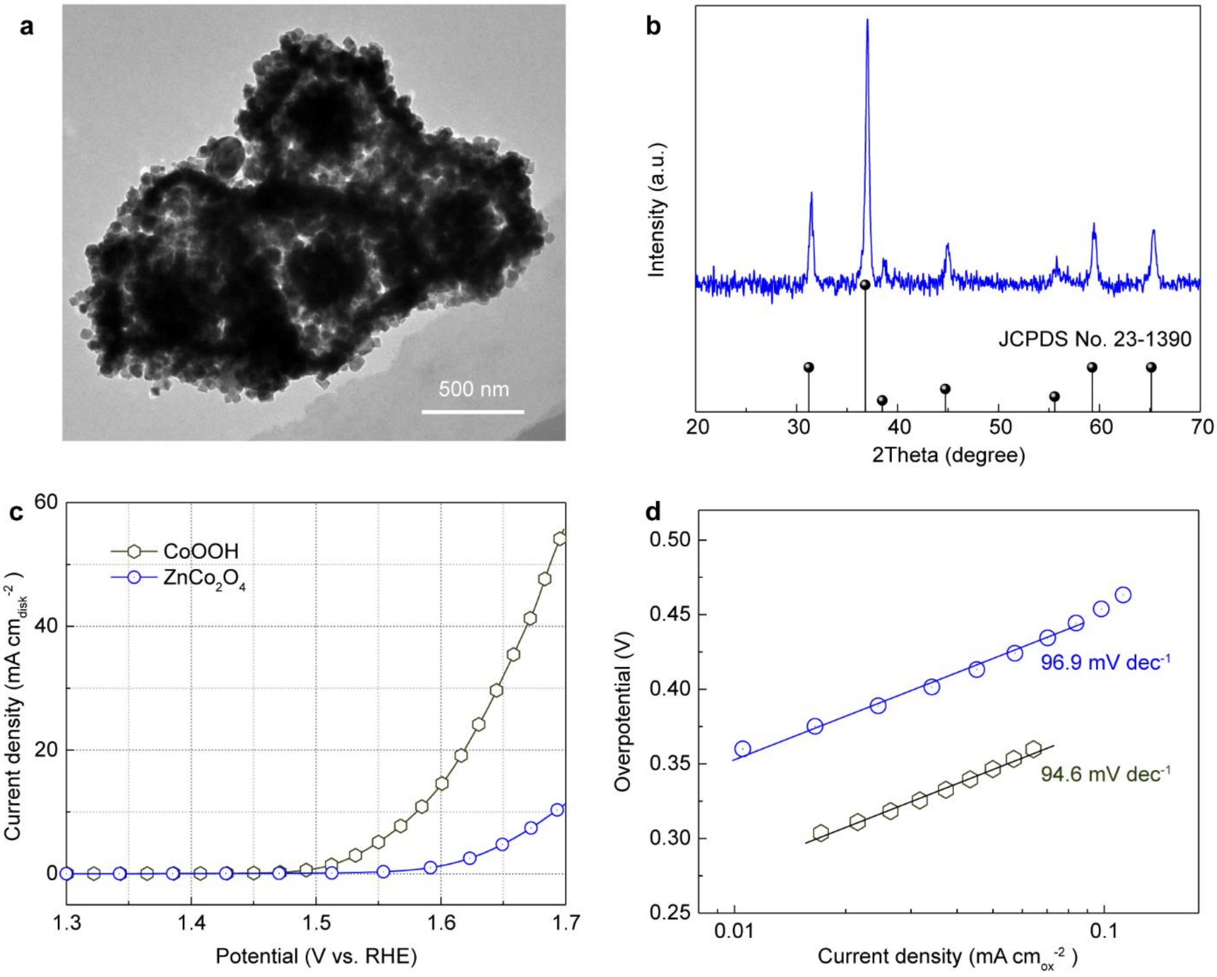

Supplementary Figure 19 | TEM image (a), XRD pattern (b), polarization curve (c) and Tafel plot of $ZnCo_2O_4$ (d). (CoOOH is used as comparison in polarization curve and Tafel plot.)

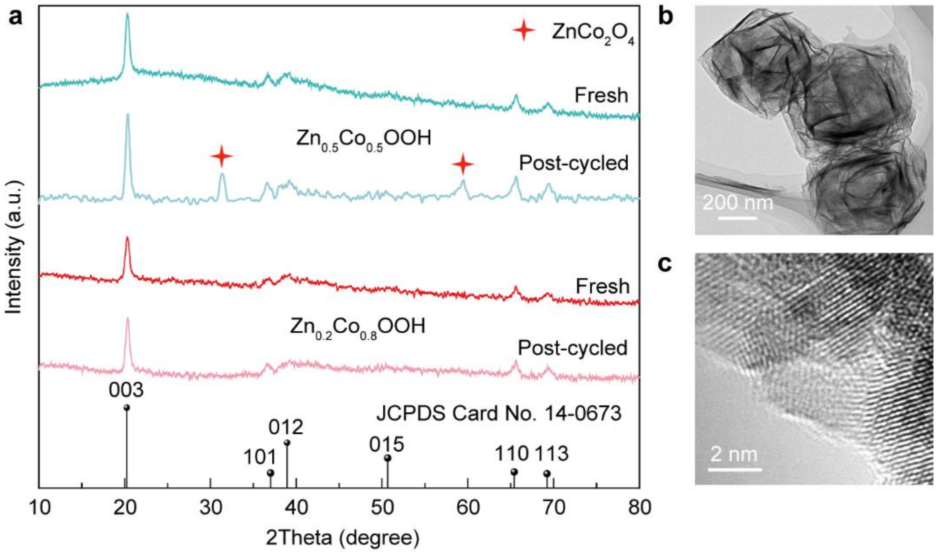

Supplementary Figure 20 | (a) XRD patterns of Zn$_x$Co$_{1-x}$OOH (x = 0.2 and 0.5) before and after OER measurement. (b) TEM and (c) HRTEM images of Zn$_{0.2}$Co$_{0.8}$OOH after OER measurement.

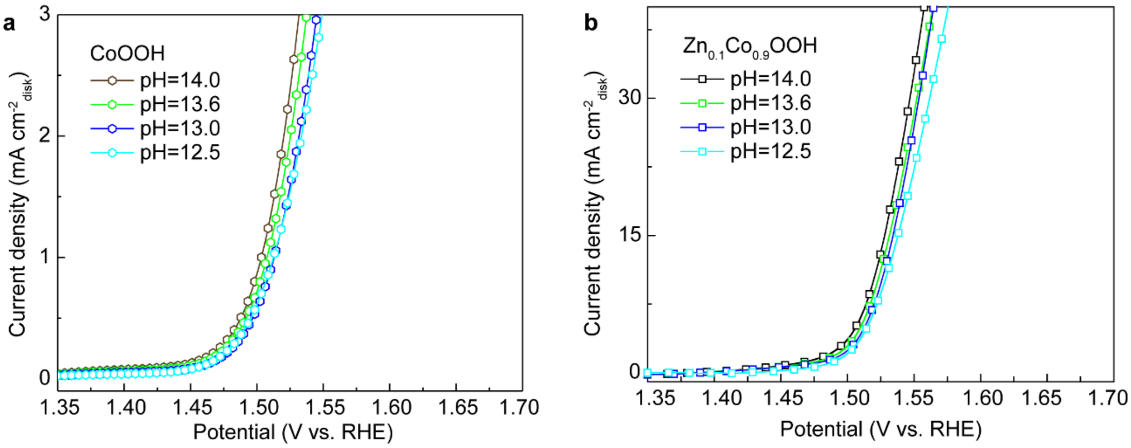

Supplementary Figure 21 | Polarization curves of CoOOH (a) and Zn$_{0.1}$Co$_{0.9}$OOH (b) at different pH (pH = 12.5 ~ 14).

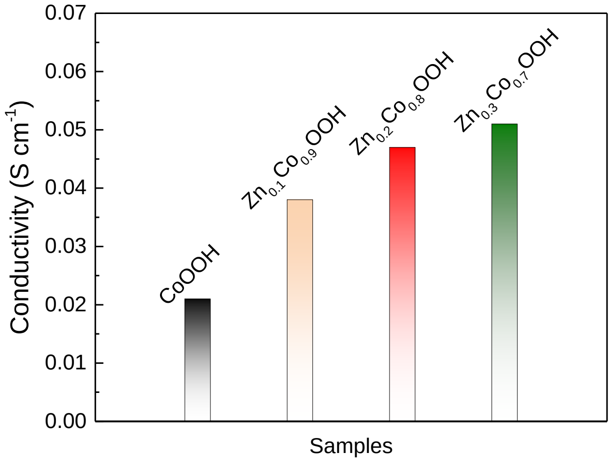

Supplementary Figure 22 | The measured electrical conductivities of CoOOH and $Zn_xCo_{1-x}OOH$.

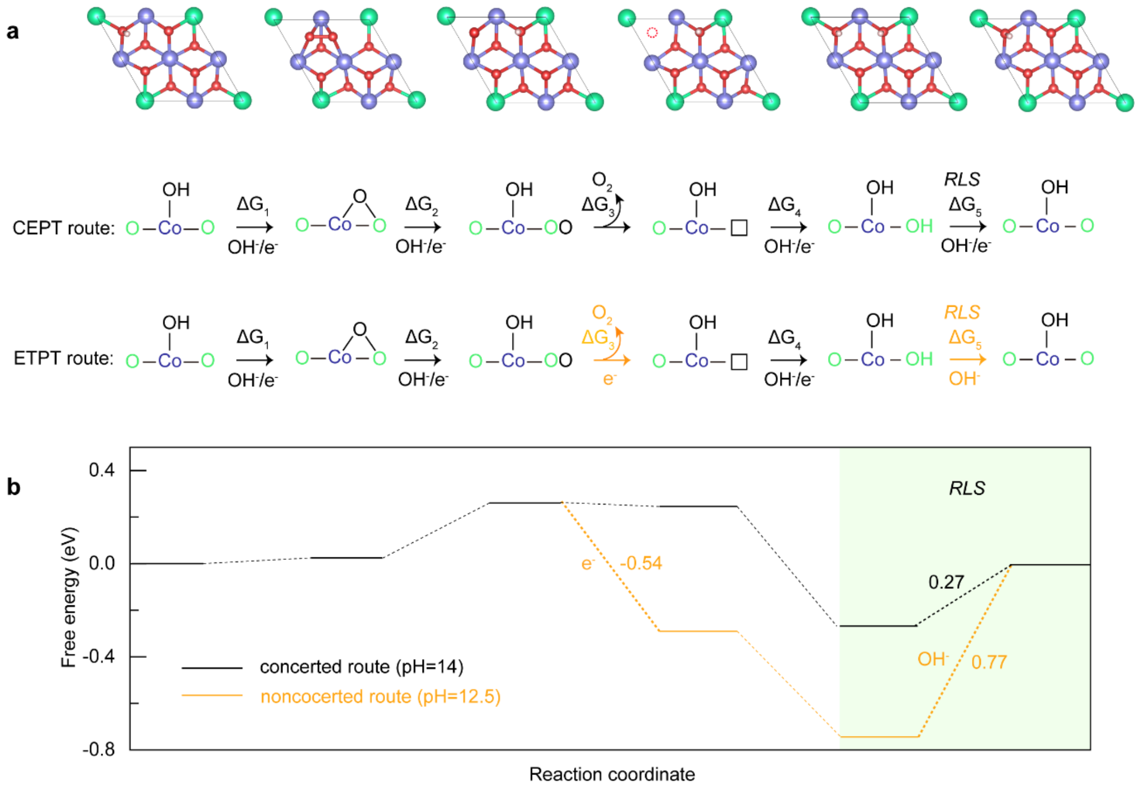

Supplementary Figure 23 | (a) Possible OER routes on $Zn_{0.2}Co_{0.8}O_2$ with LOM mechanism. (b) Free energies of OER steps via concerted and nonconcerted routes on $Zn_{0.2}Co_{0.8}O_2$, respectively.

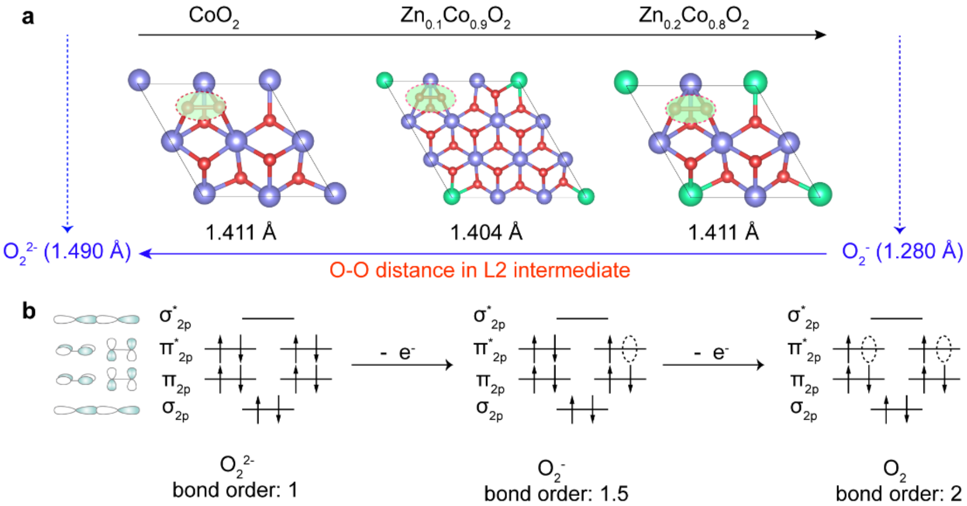

Supplementary Figure 24 | (a) O-O distance of L2 intermediate for CoO_2 and $Zn_xCo_{1-x}O_2$ (x = 0, 0.1 and 0.2) with LOM pathway. (b) Schematic electronic configuration for O_2^{2-}, O_2^- ions and O_2 gas.

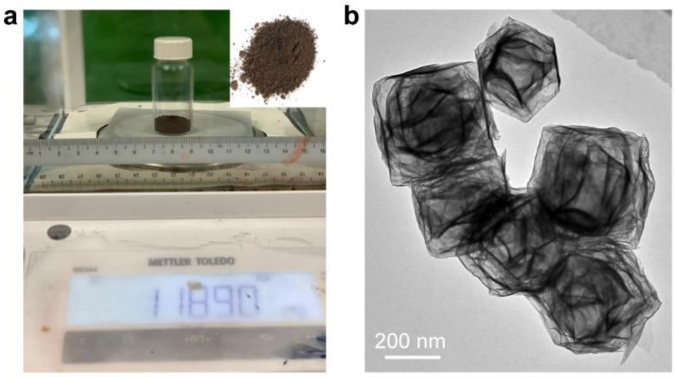

Supplementary Figure 25 | Photo of ~1.2 g of the $Zn_{0.2}Co_{0.8}OOH$ (a) and corresponding TEM image (b).

Supplementary References

1. Man, I.C., *et al.* Universality in oxygen evolution electrocatalysis on oxide surfaces. *ChemCatChem* **3**, 1159-1165 (2011).
2. Rong, X., Parolin, J., Kolpak, A.M. A fundamental relationship between reaction mechanism and stability in metal oxide catalysts for oxygen evolution. *ACS Catal.* **6**, 1153-1158 (2016).
3. Nørskov, J.K., *et al.* Origin of the overpotential for oxygen reduction at a fuel-cell cathode. *J. Phys. Chem. B* **108**, 17886-17892 (2004).
4. Doyle, A.D., Montoya, J.H., Vojvodic, A. Improving oxygen electrochemistry through nanoscopic confinement. *ChemCatChem* **7**, 738-742 (2015).